Full-coverage 1 km daily ambient $PM_{2.5}$ and O_3 concentrations of China in 2005-2017 based on multi-variable random forest model

Runmei Ma[1#], Jie Ban[1#], Qing Wang[1#], Yayi Zhang[1], Yang Yang[2], Shenshen Li[3], Wenjiao Shi[4, 5], Zhen Zhou[1,6], Jiawei Zang[1,6], Tiantian Li[1*]

[1] China CDC Key Laboratory of Environment and Population Health, National Institute of Environmental Health, Chinese Center for Disease Control and Prevention, Beijing, 100021, China

[2] Institute of Urban Meteorology, China Meteorological Administration, Beijing, 100089, China

[3] State Key Laboratory of Remote Sensing Science, Institute of Remote Sensing and Digital Earth, Chinese Academy of Sciences, Beijing, 100101, China

[4] Key Laboratory of Land Surface Pattern and Simulation, Institute of Geographic Sciences and Natural Resources Research, Chinese Academy of Sciences, Beijing 100101, China

[5] College of Resources and Environment, University of Chinese Academy of Sciences, Beijing 100049, China

[6] School of Marine Technology and Geomatics, Jiangsu Ocean University, Lianyungang 222000, China

[#] Runmei Ma, Jie Ban and Qing Wang are the co-first authors.

[*] Corresponding author: E-mail: litiantian@nieh.chinacdc.cn

Abstract

The health risks of fine particulate matter ($PM_{2.5}$) and ambient ozone (O_3) have been widely recognized in recent years. An accurate estimate of $PM_{2.5}$ and O_3 exposures is important for supporting health risk analysis and environmental policy-making. The aim of our study was to construct random forest models with high-performance, and estimate daily average $PM_{2.5}$ concentration and O_3 daily maximum of ~~8h~~ 8h-average concentration (O_3-8hmax) of China in 2005-2017 at a spatial resolution of 1km×1km. The model variables included meteorological variables, satellite data, chemical transport model output, geographic variables and socioeconomic variables. Random forest model based on ten-fold cross validation was established, and spatial and temporal validations were performed to evaluate the model performance. According to our sample-based division method, the daily, monthly and yearly ~~simulations~~ estimations of $PM_{2.5}$ from test datasets gave average model fitting R^2 values of 0.85, 0.88 and 0.90, respectively; these R^2 values were 0.77, 0.77, and 0.69 for O_3-8hmax, respectively. The meteorological variables and their lagged values can significantly affect both $PM_{2.5}$ and O_3-8hmax ~~simulation~~estimations. During 2005-2017, $PM_{2.5}$ exhibited an overall downward trend, while ambient O_3 experienced an upward trend. Whilst the spatial patterns of $PM_{2.5}$ and O_3-8hmax barely changed between 2005 and 2017, the temporal trend had spatial characteristic. The dataset is accessible to the public at https://doi.org/10.5281/zenodo.4009308 (Ma et al., 2021), and the shared data set of Chinese Environmental Public Health Tracking: CEPHT (https://cepht.niehs.cn:8282/developSDS3.html).

1 Introduction

Air pollution is becoming a main concern of modern society due to various health risks. According to the latest Global Burden of Disease (GBD) report, air pollution has caused approximately 6.67 million deaths (95% UI: 5.90-7.49 million), and ranked fourth on the global list of death-related risk factors in 2019 (Health Effects Institute, 2020; Murray et al., 2020). Ambient fine particulate matter ($PM_{2.5}$) and ambient ozone (O_3) have been identified and proven to be related to many health outcomes. China is known to be one of the countries with the most serious air pollution in the world. Strict pollution control measures (including *the Air Pollution Prevention and Control Action Plan* and *three-year action plan to fight air pollution*) were enacted by the Chinese government~~ in order~~ to control and reduce~~ serious~~ air pollution since 2013. The implementation of these measures has resulted in a markable drop of emissions and $PM_{2.5}$ concentration. ~~Nonetheless~~However, the occasional ~~haze and unsatisfactory O_3~~ pollution ~~control effects~~ events~~in 2013-2017~~, as well as the short development history of air quality monitoring network, have brought many difficulties to accurately capture the temporal and spatial patterns of $PM_{2.5}$ and O_3 concentrations. Therefore, it is difficult to develop a complete decision-making basis for handling air pollution. In addition, there are gaps in epidemiological studies linking air pollutants to health outcomes, due to the lack of accurate measurements of $PM_{2.5}$ and ambient O_3 concentrations. To this end, an accurate estimate of $PM_{2.5}$ and O_3 exposures is essential to support health risk analysis and environmental policy-making.

Suitable model variables and advanced ~~simulation~~estimation method are important to achieve accurate modeling. Basically, $PM_{2.5}$ is jointly affected by both natural conditions and human activities over space and time, e.g., Aerosol Optical Depth (AOD), meteorological conditions, geographic factors and human-related features (Wei et al., 2021). While O_3 is a secondary pollutant, which is produced by a series of complex photochemical reactions on the basis of precursor including nitrogen oxides (NOx) and volatile organic compounds (VOCs) under the action of high temperature and strong radiation. These complex characteristic puts forward higher requirements on the ability of the modeling method to handle multi-variable, and capture the non-linear relationships between variables and air pollutants. Many models have been developed to ~~simulate~~estimate the spatiotemporal distribution of $PM_{2.5}$ and O_3 concentrations in China. Machine-learning approaches (e.g., random forest (RF), extreme gradient boosting and deep belief network models) can mine useful information from a large amount of input data and explore the nonlinear relationship, ~~leading to~~bring a better performance in modeling work (Chen et al., 2018, 2019; Di et al., 2017; Li et al., 2017; Wei et al., 2019; Zhan et al., 2018). However, most of these ~~simulation~~estimation datasets cannot balance long time series and high spatiotemporal resolution. Besides, there is no long-term ~~simulation~~estimation dataset for both $PM_{2.5}$ and O_3 concentrations with high temporal and spatial resolution for supporting epidemiological research. Therefore, by incorporating multi-source data into random forest models, this study makes an attempt to ~~simulate~~estimate the high-resolution

(1km×1km) ambient $PM_{2.5}$ and O_3 concentrations of China in 2005-2017.

2. Method

The model variables of this study include meteorological variables, geographical variables, socio-economic variables, satellite data and chemical transport model output in 2013-2017. Daily average $PM_{2.5}$ and O_3 daily maximum of ~~8h~~ 8h-average concentration (O_3-8hmax) monitoring data of 1479 sites in 2013-2017 was obtained (Fig. 1; Fig. S1 and Fig. S2). A 1km×1km standard grid is created across the country (35.55° N to 43.12° N, and 112.95° E to 120.35° E) with a total of 9495025 grid cells. The coordinate system of the grid is WGS-84~~.~~; and the projection of the grid is the Albers Conical Equal Area Projection. We construct high-performance random forest (RF) models (temporal resolution: daily; spatial resolution: 1km×1km), and ~~simulate~~estimate the grid daily average $PM_{2.5}$ concentration and O_3-8hmax concentration of China in 2005-2017.

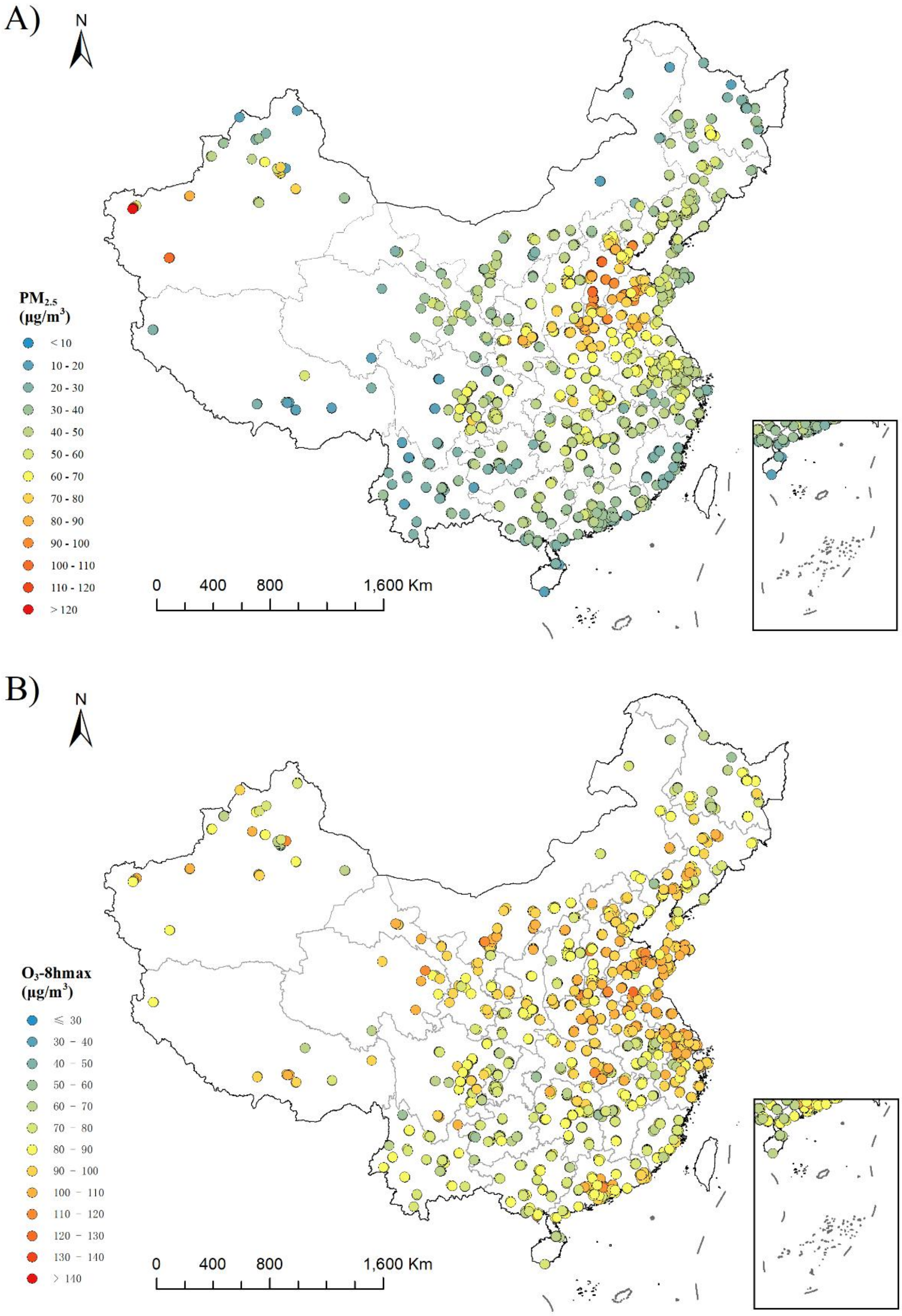

Fig.1 Station distribution in China and average ground monitoring concentration based on the available data of $PM_{2.5}$ (A) and O_3-8hmax (B) from 2013 to 2017~~Station distribution in China and average ground monitoring concentration of $PM_{2.5}$ (A) and O_3-8hmax (B) from 2013 to 2017~~

2.1 Data set

The model variables used in this study mainly include Aqua AOD~~ (Aerosol Optical Depth)~~ for $PM_{2.5}$ modeling, GEOS-Chem chemical transport model output for O_3 modeling, and some variables shared by $PM_{2.5}$ and O_3: 13 meteorological variables (includes boundary layer height, surface pressure, 2 meter dew point temperature, evaporation, albedo, low cloud cover, medium cloud cover, high cloud cover, total precipitation, 10 meter U wind component, 10 meter V wind component, 2 meter surface temperature and surface solar radiation downwards) and its lag 1 and lag 2, geographic and socio-economic variables, such as Digital Elevation Model~~DEM~~ (DEM~~Digital Elevation Model~~), Normalized Difference Vegetation Index~~NDVI~~ (NDVI~~Normalized Difference Vegetation Index~~), population, Gross Domestic Product~~GDP~~ (GDP~~Gross Domestic Product~~), road network and dummy variables (includes season, month, and spatial dummy variables, province). A more detailed description of the model variables is given in Table S1. The processing method has been described in detail in our earlier studies (Ma et al., 2021; Zhao et al., 2019). Briefly, most of the model variables are processed into 1km×1km resolution based on the standard grid using interpolation methods (such as inverse distance weighted and bilinear algorithm) in ArcGIS 10.2 and Python 2.7. For example, AOD is processed by ENVI 5.3+IDL and extracted into standard grid using ArcPy, then the inverse distance weighted interpolation is carried out to obtain the 1km×1km resolution data. For the long-term variables, the corresponding monthly and annual level value is assigned to each day. Subsequent modeling work was carried out based on the data set that covering monitoring data and all variables.

2.2 Random forest model

Random forest is an ensemble machine learning method consisting of many individual decision trees growing from bagged data and its prediction is a vote result of those trees (Breiman, 2001). The RF algorithm primarily integrates learning principles, trains several individual learners, and finally forms a strong learner through a certain combination strategy; through multiple rounds of training, multiple prediction results are obtained, and the final results are obtained after average aggregation.

The random forest models are established using the 10-fold cross validation method. First~~ of all~~, this method randomly divides the modeling data set into 10 parts; then 9 of them are used for modeling, the remaining one is used for ~~simulation~~estimation and be compared with observations. The verification is repeated until every part is predicted. In this way, the modeling and verification of ~~simulation~~estimation are repeated 10 times in total, and the average values of the 10 runs is took as the final result, i.e., the CV-R^2. The formulae of the models are as follows:

$$PM_{2.5i,j} = f(METE_{i,j},\ lag1METE_{ij},\ lag2METE_{i,j}, AOD_{i,j},\ LD_j,\ ROAD_j,\ NDVI_j,\ ELE_j,\ GDP_j,\ POP_j,\ SEASON_i,\ MON_i,\ PRO_j) \quad (1)$$

$$O_3\text{-}8hmax_{i,j} = f(METE_{i,j},\ lag1METE_{ij},\ lag2METE_{i,j}, GEOS_{i,j},\ LD_j,\ ROAD_j,\ NDVI_j,\ ELE_j,$$

$GDP_j, POP_j, SEASON_i, MON_i, PRO_j)$

(2)

where $PM_{2.5\ i,j}$ and $O_3\text{-}8hmax_{i,j}$ are the $PM_{2.5}$ and O_3-8hmax concentrations on day i in grid cell j; $METE_{i,j}$ is 13 meteorological variables on day i in grid cell j, and lag 1 $METE_{i,j}$ and lag2 $METE_{i,j}$ represent corresponding one-day lag and two-day lag values, respectively; $GEOS_{i,j}$ and $AOD_{i,j}$ are the GEOS-Chem model output and AOD value on day i in grid cell j; LD_j, $ROAD_j$, $NDVI_j$, ELE_j, GDP_j and POP_j are the land use coverage, length of a variety of roads, NDVI, elevation, GDP and population in grid cell j, respectively; $SEASON_i$, MON_i and PRO_j are the season and month of day i, and province of grid cell j, respectively.

In general, the random forest parameters that need to be adjusted include n_estimators (number of decision trees) and the max_depth (maximum depth of the trees). Unlike the previous methods of manually adjusting parameters, the parameters of random forest were optimized using GridSearchCV, which can realize cross-validated grid-search over a parameter grid. After GridSearchCV, we set max_depth as 36 and n_estimators as 200 for $PM_{2.5}$ modeling. For O_3-8hmax modeling, we set max_depth as 54 and n_estimators as 200.

2.3 Validation method

To comprehensively verify the model performance, we construct the main models using sample-based division method. Models using spatial-based and temporal-based division method are further construct to test the model performance in spatial and temporal scale.

The data set was randomly divided into training set (90% of the records) and test set (10% of the records) by using the sample-based division method. We construct the main model using the training set with a 10-fold cross-validation. Since the data in the test set is not used in the main model, "true model performance" can be verified. The coefficient of determination (R^2) of main model on test set (test-R^2), and the verification indicators of model uncertainty, the root mean square error (RMSE) and mean absolute error (MAE) are calculated for the $PM_{2.5}$ and O_3-8hmax model, ~~respetively~~respectively. The monthly and yearly test-R^2 are also calculated.

For the spatial verification, 90% of the monitoring stations are randomly selected. The monitoring data of these stations is used as the training set, and the monitoring data of remaining stations is used as the testing set. For the temporal verification, all date in 2013-2017 is randomly divided into nine and one, and the data in theses dates is used as training and test sets, respectively. After that, the test-R^2, RMSE and MAE are calculated.

2.4 ~~Simulation~~Estimation of daily $PM_{2.5}$ and ambient O_3 of China from 2005 to 2017

Based on the final models of $PM_{2.5}$ and O_3-8hmax, we ~~simulate~~estimate the gridded daily average $PM_{2.5}$ concentration and O_3-8hmax concentration of China in 2005-2017. The spatial pattern and temporal trend of $PM_{2.5}$ and O_3-8hmax concentrations are analyzed, and compared with other modeling products.

The modeling and ~~simulation~~estimations are performed in Python 2.7.13 using the scikit-learn-0.20.3 and GridSearchCV packages. The workflow of this study is displayed in Fig. 2.

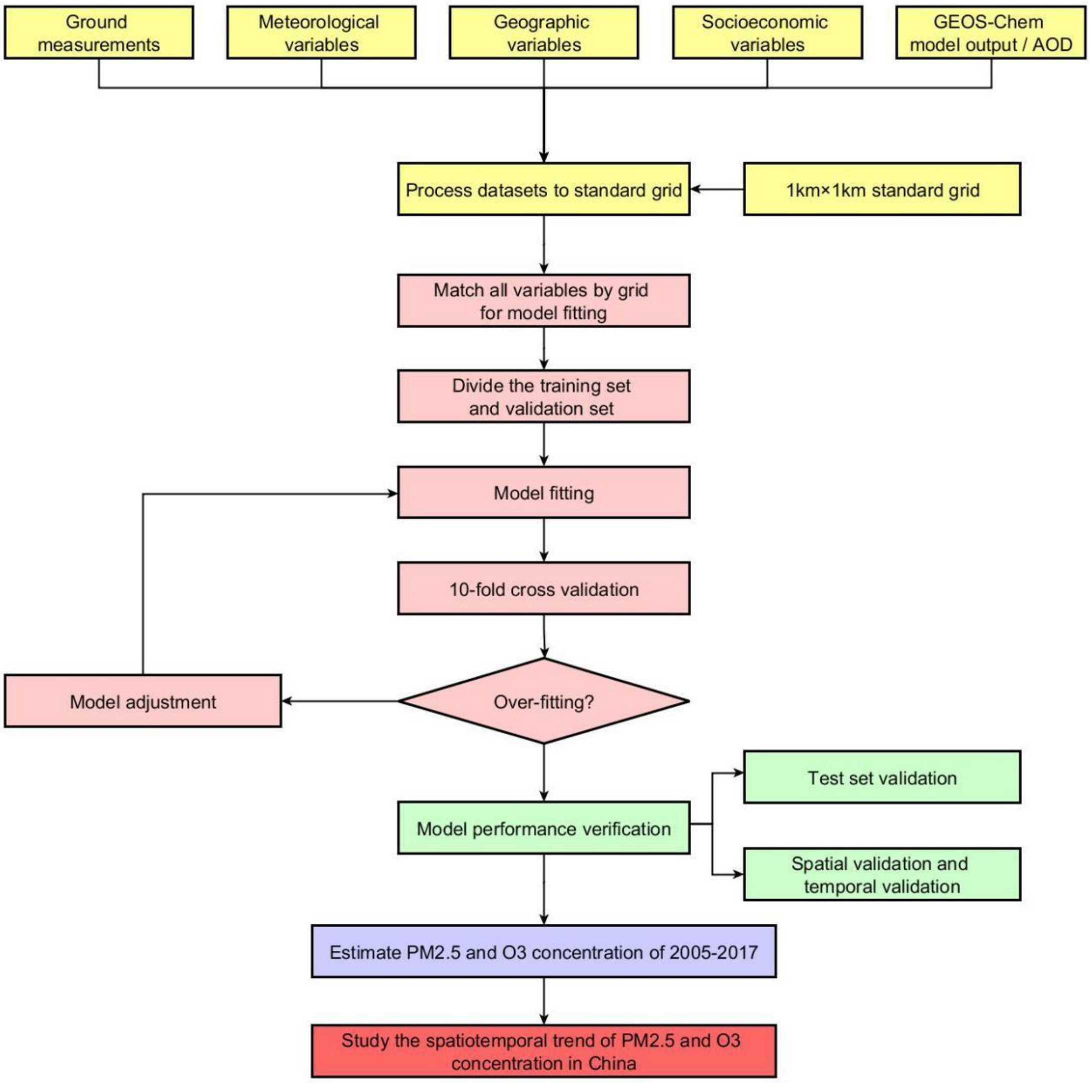

Fig. 2 The workflow of modeling process in the study

3 Results and Discussion

A total of 981744 monitoring data records were used in the final model-fitting data set. The mean ± standard deviation of $PM_{2.5}$ and ambient O_3 concentrations in 2013-2017 were 59.60 ± 45.85 μg/m^3 and 86.72 ± 47.73 μg/m^3, respectively. The results of descriptive analysis for variables included in $PM_{2.5}$ and O_3-8hamx model is shown in Table S2.

3.1 Model fitting and validation

The cross-validation results indicate that the ~~simulate~~estimated $PM_{2.5}$ and O_3-8hmax concentrations matched reasonably with the observed $PM_{2.5}$ and O_3-8hmax concentrations, with high fitted test-R^2 values. According to our sample-based division method, the test-R^2 values of the ~~simulate~~estimated daily, monthly and yearly $PM_{2.5}$ concentrations were 0.85, 0.88 and 0.90, respectively (Fig. 3). Likewise, the test-R^2 values of the ~~simulate~~estimated daily, monthly and yearly O_3-8hmax concentrations were 0.77, 0.77 and 0.69, respectively (Fig. 4). The RMSE and MAE for $PM_{2.5}$ in daily level were 17.72 and 9.37 μg/m^3; for O_3-8hmax, the values were 23.10 and 15.43 μg/m^3. The model performance is comparable to previous studies (Di et al., 2017; Li and Cheng, 2021; Liu et al., 2020; Wei et al., 2021, 2020, 2019). At provincial/city level, The model performance of $PM_{2.5}$ ~~simulation~~estimations of Shanghai, Beijing, Hubei, Hebei and Sichuan ranked the top 5 with relatively high test-R^2 ($\geq$0.90), while those of Tibet, Qinghai, Gansu, Anhui and Yunnan were less accurate with relatively low test-R^2 values (<0.70). The model performance of O_3-8hmax ~~simulation~~estimations of Beijing, Chongqing, Shanghai, Tianjin and Henan ranked the top 5 with relatively high test-R^2 values (≥0.83), while those of Gansu, Anhui, Heilongjiang, Guizhou and Tibet were poorer with relatively low test-R^2 values (<0.62) (Table S3).

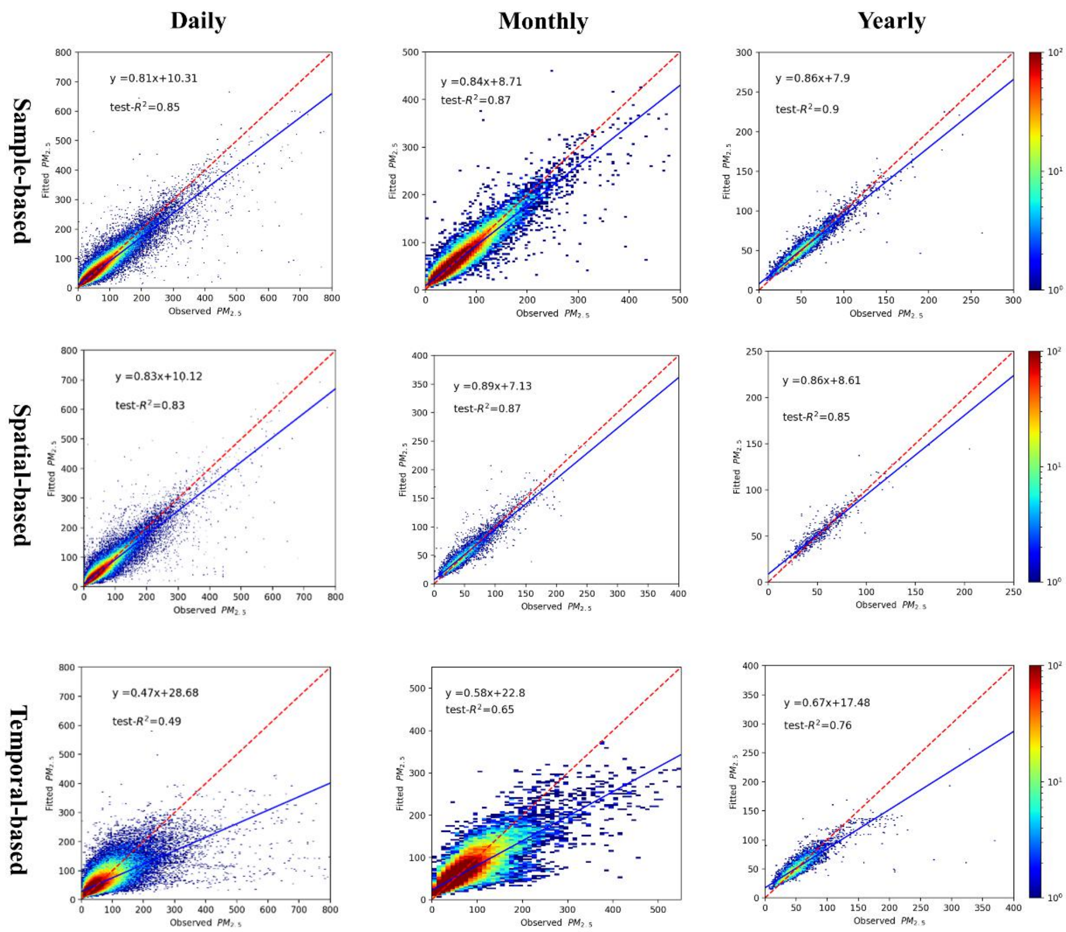

Fig. 3 The density plot of $PM_{2.5}$ model

From left to right is different temporal scale: daily, monthly and yearly; From top to bottom is different validation method: sample-based, spatial-based and temporal-based.

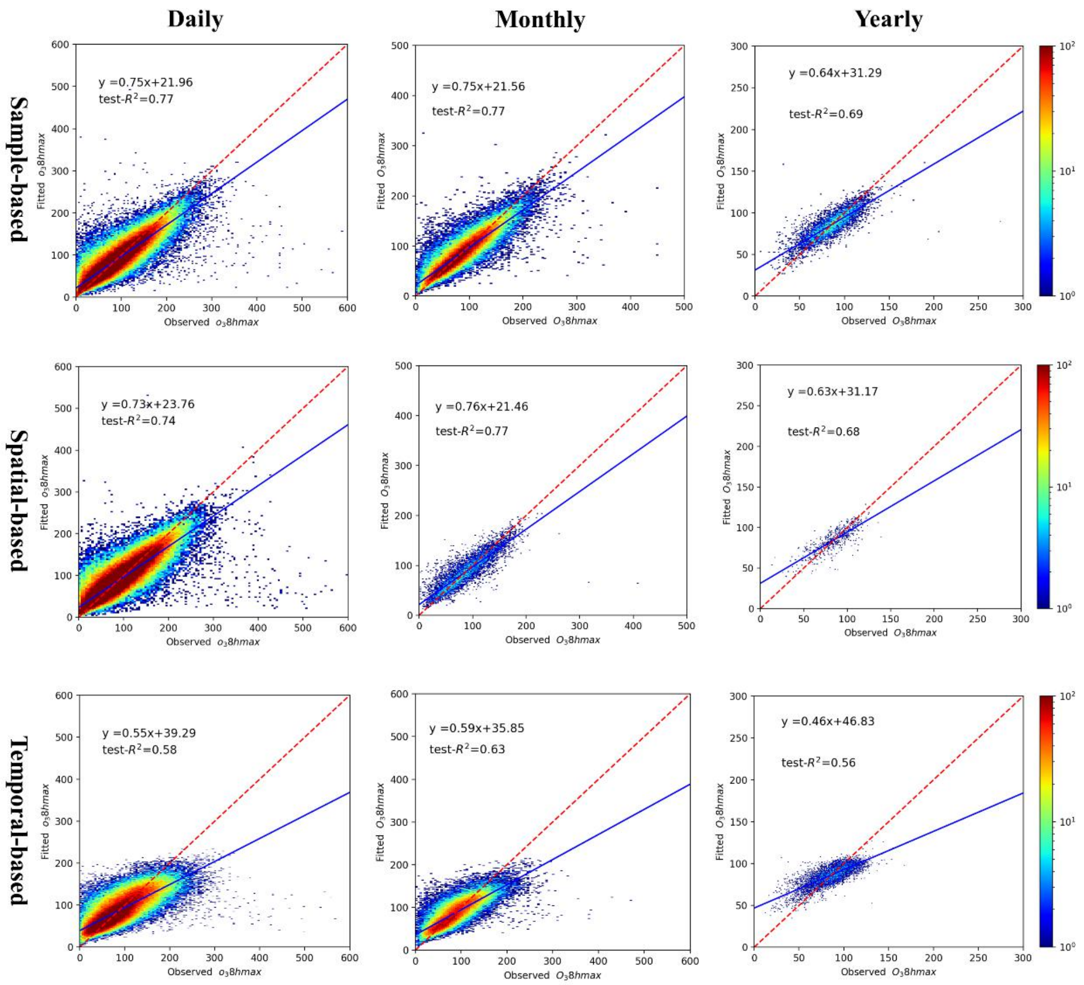

Fig. 4 The density plot of O_3-8hmax model

From left to right is different temporal scale: daily, monthly and yearly; From top to bottom is different validation method: sample-based, spatial-based and temporal-based.

The spatial and temporal test-R^2 of our models explained the uncertainty ~~of the models~~ to some content (Fig. 3 and Fig. 4). The spatial test-R^2 values for daily, monthly and yearly $PM_{2.5}$ ~~simulation~~estimation were 0.83, 0.87 and 0.~~86~~85, respectively; while those of daily, monthly and yearly O_3-8hmax ~~simulation~~estimations were 0.74, 0.77 and 0.68, respectively. The relatively high spatial test-R^2~~performance~~ demonstrates the reasonable performance of our models in areas without monitoring stations. The temporal test-R^2 values of daily, monthly and yearly $PM_{2.5}$ ~~simulation~~estimations were 0.49, 0.65 and 0.76, respectively; while those of daily, monthly and yearly O_3-8hmax ~~simulation~~estimations were 0.58, 0.63 and 0.56, respectively. These results indicate the uncertainty of our models when modeling data in historical period, although the performance is among the best compared with previous studies. The simulation accuracy is a universal issue in the present studies of air pollutant concentrations in historical period without monitoring data. Further efforts are need to improve the model performance of historical estimations.

3.2 Feature importance

The feature importance of the variables in our random forest models is presented in Table S4-1 and S4-2. Similar to previous studies (Chen et al., 2018; Zhan et al., 2018), the meteorological factors and their lagged values can significantly affect both $PM_{2.5}$ and O_3-8hmax modeling. Moreover, the specific features for $PM_{2.5}$ and O_3, AOD and GEOS-Chem output, also demonstrated high importance in modeling work.

For $PM_{2.5}$ modeling work (Table S4-1), the meteorological variables (boundary layer height, evaporation, 2 meter dew point temperature) and its lagged effect were among the top ten important factors, totaling 33.6% in modeling work. The lagged effects greatly contributed to $PM_{2.5}$ modeling. For example, the lag1 boundary layer height ranked first (17.2%) in our study, which is similar to previous studies (Zhao et al., 2019). The interpolated AOD (5.6%), DEM (4.9%) and season (3.7%) also demonstrated high importance, which showed crucial effects of satellite data, terrain distribution characteristics in the study area, and study period on $PM_{2.5}$ modeling. The relative contribution of land-use, NDVI, population density, road length and GDP are negligible (the importance scores less than 1%). Unlike DEM, these factors are subjected to the influence of socioeconomic status in study area. In the future study, the integration of these factors with a higher temporal resolution might change its contribution to the ~~simulation~~estimation.

The feature importance of ambient O_3 is consistent with its formation and dissipation mechanism: surface solar radiation downwards and its lagged effect according for 3~~8.07~~9.2% in modeling work (Table S4-2). Other meteorological factors (2 meter temperature, boundary layer height, 10 meter V wind component, and low cloud cover) according for totaling 9.54% importance scores. Our analysis also suggests the high importance of GEOS-Chem model (7.24%), altitude (1.~~88~~9%), and dummy factors including year (2.~~17~~2%) and province (1.~~56~~6%) in O_3 modeling. By contrast, the relative contribution of land-use, NDVI and road length are negligible (the importance scores less than 1%). The high importance rank of population and GDP might be attributed to the relatively high sensitivity of O_3 to anthropogenic emission sources (compared to $PM_{2.5}$).

3.3 The spatial characteristics and temporal trend of $PM_{2.5}$ and ambient O_3 of China from 2005 to 2017

During 2005-2017, $PM_{2.5}$ showed an overall downward trend, while ambient O_3 showed an upward trend in recent years (Fig. 5, Fig. ~~S1~~ S3-S~~and Fig. S2~~6). Relative to 2005, $PM_{2.5}$ concentration has increased by 2.60 μg/m^3 in 2013. Nevertheless, after the implementation of the *Air Pollution Prevention and Control Action Plan*, a strict pollution control measure, $PM_{2.5}$ concentration has declined by 11.041 μg/m^3 in 2017 (relative to 2013). This has resulted in a downward trend of $PM_{2.5}$ concentration in 2005-2017: $PM_{2.5}$ concentration in 2017 has decreased by 8.44 μg/m^3 relative to 2005 (Fig. 5 and Fig. ~~S1~~S3). In key pollution areas, with the implementation of various air pollution prevention and control policies, $PM_{2.5}$ levels in the Beijing-Tianjin-Hebei region have dropped the most, but the overall– concentration levels are still higher than those in the Yangtze River Delta and Pearl River Delta (Fig. S4). For O_3-8hmax, upward barely changed. Relative to 2005, O_3-8hmax concentrations in 2013 and 2017 have increased by 0.39 μg/m^3 and 7.83 μg/m^3, respectively. The upward trend during 2005-2017 was mostly due to the significant changes between 2013 and 2017: relative to 2013, the O_3-8hmax concentration has increased by 7.44 μg/m^3 in 2017 (Fig. 5 and Fig. ~~S2~~S5). The Beijing-Tianjin-Hebei ~~region have~~region has shown an obvious upward trend since 2013; while the Pearl River Delta region change trend is not obvious (Fig. S6). During the strict pollution control period, VOC emissions were not effectively controlled could be one of the main reasons. Therefore, integrated management of VOCs and NOx in key industries and areas is important.

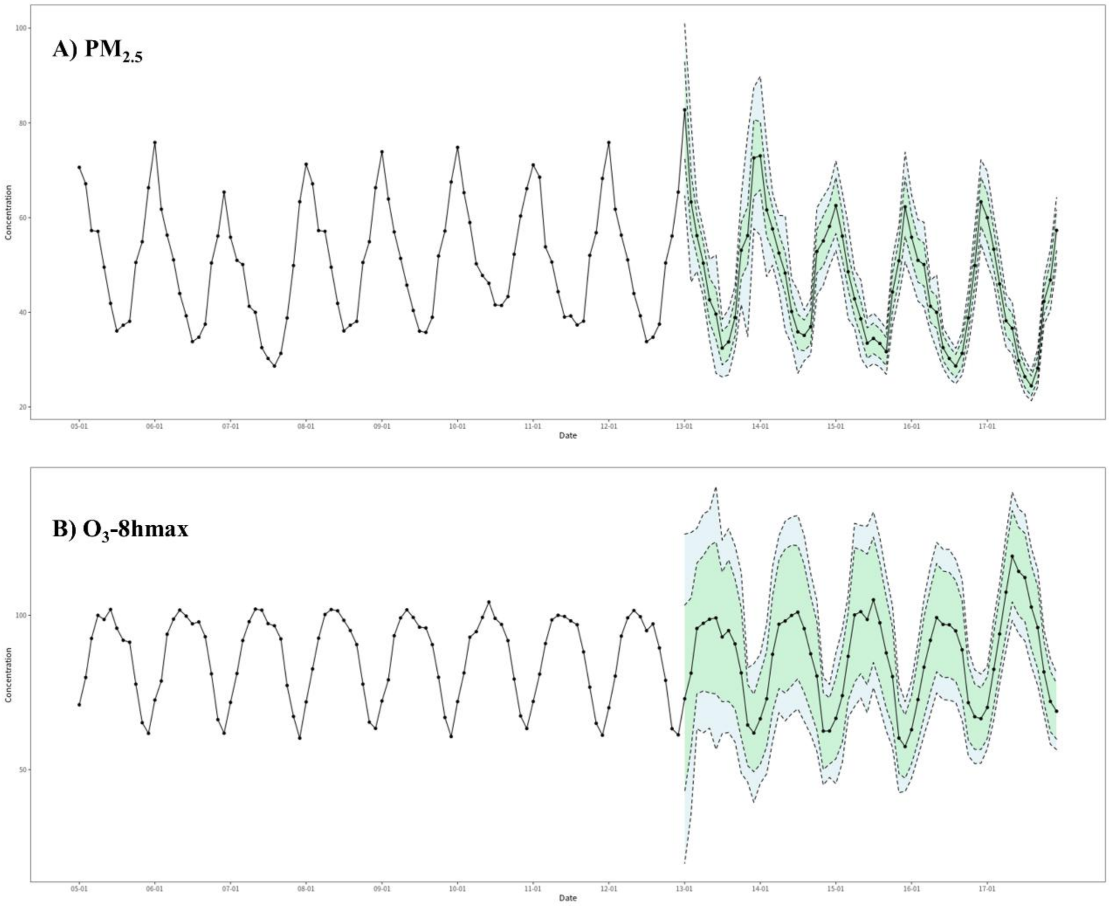

Fig.5 The temporal trend of $PM_{2.5}$ and O_3-8hmax concentration in China from 2005-2017

The black dots represent the monthly average $PM_{2.5}$ and O_3-8hmax concentration from 2005 to 2017, the blue color band represents the range of the monthly average $PM_{2.5}$ and O_3-8hmax concentration plus or minus the RMSE value from 2013-2017 (period with monitoring data), and the green color band represents the range of the monthly average $PM_{2.5}$ and O_3-8hmax concentration plus or minus the MAE value from 2013-2017 years.

The seasonal distributions of $PM_{2.5}$ and O_3-8hmax concentrations were obvious during 2005-2017 (Fig. ~~S3~~ S7 and Fig. ~~S4~~S8). The lowest seasonal $PM_{2.5}$ concentration occurred in summer, with an average concentration of 33.6 ± 11.39μg/m^3; and the highest seasonal $PM_{2.5}$ concentration occurred in winter, with an average concentration of 57.4±21.76μg/m^3. In winter, temperature inversion occurs frequently, and the thickness of the mixed layer is low, which is not conducive to the diffusion of pollutants, which leads to the accumulation of $PM_{2.5}$ near the ground (Sun et al, 2014). In opposite, the lowest seasonal O_3-8hmax concentration was in winter, with an average concentration of 72.65±6.28μg/m^3; The highest seasonal O_3-8hmax concentration was in summer, with an average concentration of 97.44±13.58μg/m^3. Temperatures and solar radiation conditions in summer increase the incidence of severe O_3 pollution events, which is consistent with its formation and dissipation mechanism.

The $PM_{2.5}$ concentrations in Beijing-Tianjin-Hebei, Chengdu-Chongqing and Xinjiang regions are higher than other regions, followed by the central China. The $PM_{2.5}$ concentrations in the southwestern regions (Yunnan and Tibet) and western part of Sichuan Province, are the lowest, followed by the inner-north regions and the south and southeastern regions (Fig. 6 ~~and~~, Fig. ~~S1~~S3 and Fig. S4; Table S5). The O_3-8hmax concentrations in the Bohai Rim, Yangtze River Delta, Pearl River Delta and other economically developed regions, southern Xinjiang, Inner Mongolia, and northeastern Gansu are relatively high (Fig. 6 ~~and~~, Fig. ~~S2~~S5 and Fig.6; Table S5). This spatial pattern barely changed during 2005-2017 (Fig. ~~S1~~ S3 and Fig. ~~S2~~S5), but the temporal trend showed spatial characteristic (Fig. 6; Fig. S4 and S6). For $PM_{2.5}$ concentration, the ~~above-mentioned~~ key pollution areas were severely polluted during 2005-2013. The air pollution control measures of these regions were strict during 2013-2017, thus the decline was obvious, especially for the Beijing-Tianjin-Hebei region. For O_3-8hmax concentration, the growth rate was not obvious (except for the eastern part of Hubei Province) during 2005-2013. However, after 2013, there was a clear upward trend across the country, especially in the northern China.

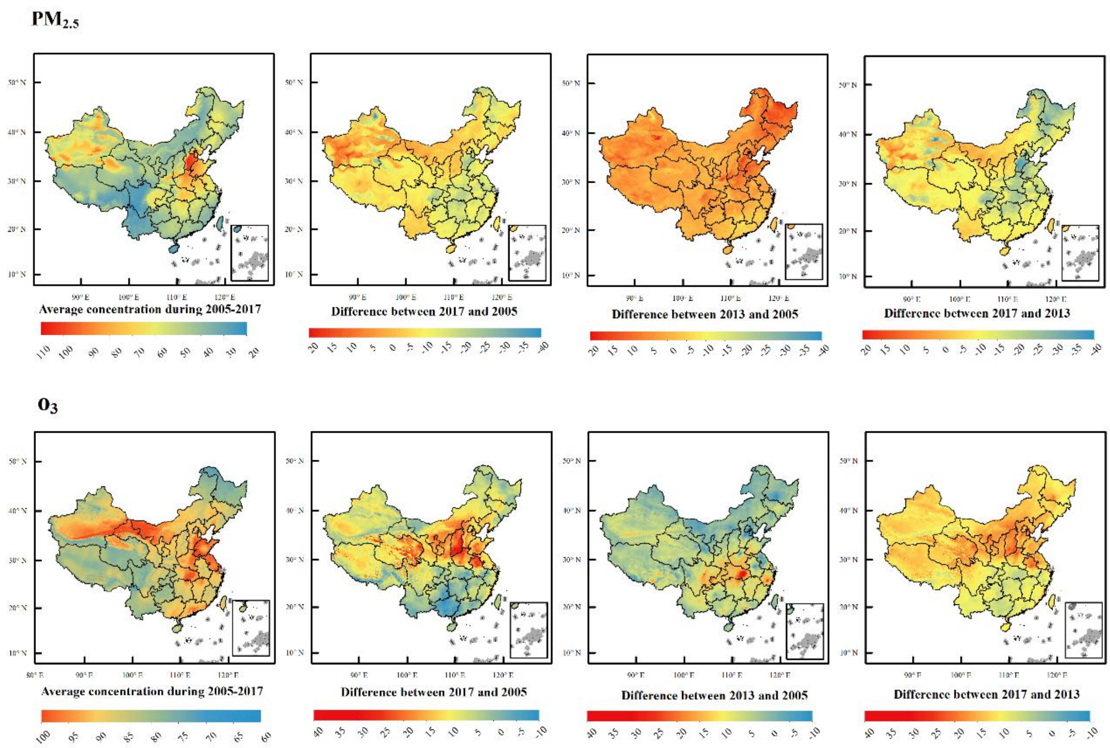

Fig. 6 ~~Simulate~~Estimated annual mean and difference of $PM_{2.5}$ and O_3-8hmax concentration in China during 2005 to 2017

The first row is maps of $PM_{2.5}$ related indicators, and the second row is maps of O_3-8hmax related indicators. From left to right are average concentration during 2005-2017, the difference between 2017 and 2005, the difference between 2013 and 2005, and the difference between 2017 and 2013.

3.4 Evaluation of the $PM_{2.5}$ and O_3 concentration products with comparison with other products

Our ~~simulation~~estimation datasets include the $PM_{2.5}$ and O_3-8hmax concentration data of China in 2005-2017 with a spatial resolution of 1km×1km resolution. With high spatial and temporal resolutions, our validation results are comparable with other modeling work (see Table S6). Considering the future application in epidemiological research, our ~~simulation~~estimation datasets would be useful: for acute effects studies, the high spatial resolution would effectively reduce exposure errors; for chronic effects studies, long-term exposure data is essential for the development of cohort studies.

Nevertheless, our ~~simulation~~estimation datasets also contain some limitations. First, we did not use emission data in our model limited by coarse resolution. However the newly published ~~The~~ high-resolution emission inventory of China ~~is made accessible to the public~~ (http://meicmodel.org/) ~~and it can~~may be utilized in future ~~simulation~~estimation studies to improve accuracy. Second, our modeling still has spatial and temporal uncertainties. In areas where monitoring sites are sparsely distributed, such as western China, it may be difficult to accurately capture the association between air pollution concentrations and variables. The model validation of historical period is also limited. Third, the interpolation process of model features inevitably introduces ~~some errors~~systematic errors. Therefore, more high-quality and high-resolution basic data would be needed in the future.

4 Data availability

The ~~simulate~~estimated $PM_{2.5}$ and O_3 data are freely accessible at https://doi.org/10.5281/zenodo.4009308 (Ma et al., 2021), and the shared data set of Chinese Environmental Public Health Tracking: CEPHT (https://cepht.niehs.cn:8282/developSDS3.html).

5 Conclusions

We constructed random forest models for simulating of daily average $PM_{2.5}$ and O_3-8hmax concentrations of China during 2005-2017, with referential feature list and comparable model performance. The ~~simulation~~estimation dataset would be useful for supporting both long-term and short-term epidemiological studies. The model can be further used for simulating daily concentrations of longer time period. The key findings are summarized as follows. First, RF model proved its superiority in our study and can be further used in the future ~~simulation~~estimation of air pollutant concentration. Second, meteorological data is the most sensitive to $PM_{2.5}$ and O_3 modeling. For $PM_{2.5}$ modeling work, boundary layer height, evaporation, 2 meter dew point temperature and its lagged effects showed the highest sensitivity. For O_3 modeling work, surface solar radiation downwards and its lagged effect were the most sensitive. Third, $PM_{2.5}$ concentration has trended downward in China, and the key polluted areas during 2005-2013 were effectively controlled during 2013-2017. O_3 concentration has trended upward in China, especially in the northern China during 2013-2017.

Author Contribution

Runmei Ma, Jie Ban and Qing Wang: Software, Investigation, Validation, Formal analysis, Data curation, Writing - original draft. Yayi Zhang: Formal analysis, Visualization. Yang Yang, Shenshen Li and Wenjiao Shi: Methodology, Writing - Review & Editing. Tiantian Li: Conceptualization, Methodology, Writing - Review & Editing.

Competing Interests

The authors declare that they have no conflict of interest.

Acknowledgements

This work was funded by grants from National Natural Science Foundation of China (Grant No. 92043301 and 42071433).

Reference

Breiman, L., 2001. Random forest. Machine Learning 45, 5–32.

Chen, G., Li, S., Knibbs, L.D., Hamm, N.A.S., Cao, W., Li, T., Guo, J., Ren, H., Abramson, M.J., Guo, Y., 2018. A machine learning method to estimate PM2.5 concentrations across China with remote sensing, meteorological and land use information. Science of The Total Environment 636, 52–60. https://doi.org/10.1016/j.scitotenv.2018.04.251

Chen, Z.-Y., Zhang, T.-H., Zhang, R., Zhu, Z.-M., Yang, J., Chen, P.-Y., Ou, C.-Q., Guo, Y., 2019. Extreme gradient boosting model to estimate PM2.5 concentrations with missing-filled satellite data in China. Atmospheric Environment 202, 180–189. https://doi.org/10.1016/j.atmosenv.2019.01.027

Di, Q., Rowland, S., Koutrakis, P., Schwartz, J., 2017. A hybrid model for spatially and temporally resolved ozone exposures in the continental United States. Journal of the Air & Waste Management Association 67, 39–52. https://doi.org/10.1080/10962247.2016.1200159

Health Effects Institute, 2020. State of Global Air 2020 28.

Li, T., Cheng, X., 2021. Estimating daily full-coverage surface ozone concentration using satellite observations and a spatiotemporally embedded deep learning approach. International Journal of Applied Earth Observation and Geoinformation 101, 102356. https://doi.org/10.1016/j.jag.2021.102356

Li, T., Shen, H., Yuan, Q., Zhang, X., Zhang, L., 2017. Estimating Ground-Level PM $_{2.5}$ by Fusing Satellite and Station Observations: A Geo-Intelligent Deep Learning Approach: Deep Learning for PM $_{2.5}$ Estimation. Geophys. Res. Lett. 44, 11,985-11,993. https://doi.org/10.1002/2017GL075710

Liu, R., Ma, Z., Liu, Y., Shao, Y., Zhao, W., Bi, J., 2020. Spatiotemporal distributions of surface ozone levels in China from 2005 to 2017: A machine learning approach. Environment International 142, 105823.

https://doi.org/10.1016/j.envint.2020.105823
Ma, R., Ban, J., Wang, Q., Zhang, Y., Li, T., 2021. Full-coverage 1 km daily ambient PM2.5 and O3 concentrations of China in 2005-2017 based on multi-variable random forest model.
Ma, R., Ban, J., Wang, Q., Zhang, Y., Li, T., 2021. Random Forest Model based Fine Scale Spatiotemporal O3 Trends in the Beijing-Tianjin-Hebei region in China, 2010 to 2017. Environmental Pollution 116635.
Murray, C.J.L., Aravkin, A.Y., Zheng, P., Abbafati, C., Abbas, K.M., Abbasi-Kangevari, M., Abd-Allah, F., Abdelalim, A., Abdollahi, M., Abdollahpour, I., Abegaz, K.H., Abolhassani, H., Aboyans, V., Abreu, L.G., Abrigo, M.R.M., Abualhasan, A., Abu-Raddad, L.J., Abushouk, A.I., Adabi, M., Adekanmbi, V., Adeoye, A.M., Adetokunboh, O.O., Adham, D., Advani, S.M., Agarwal, G., Aghamir, S.M.K., Agrawal, A., Ahmad, T., Ahmadi, K., Ahmadi, M., Ahmadieh, H., Ahmed, M.B., Akalu, T.Y., Akinyemi, R.O., Akinyemiju, T., Akombi, B., Akunna, C.J., Alahdab, F., Al-Aly, Z., Alam, K., Alam, S., Alam, T., Alanezi, F.M., Alanzi, T.M., Alemu, B. wassihun, Alhabib, K.F., Ali, M., Ali, S., Alicandro, G., Alinia, C., Alipour, V., Alizade, H., Aljunid, S.M., Alla, F., Allebeck, P., Almasi-Hashiani, A., Al-Mekhlafi, H.M., Alonso, J., Altirkawi, K.A., Amini-Rarani, M., Amiri, F., Amugsi, D.A., Ancuceanu, R., Anderlini, D., Anderson, J.A., Andrei, C.L., Andrei, T., Angus, C., Anjomshoa, M., Ansari, F., Ansari-Moghaddam, A., Antonazzo, I.C., Antonio, C.A.T., Antony, C.M., Antriyandarti, E., Anvari, D., Anwer, R., Appiah, S.C.Y., Arabloo, J., Arab-Zozani, M., Ariani, F., Armoon, B., Ärnlöv, J., Arzani, A., Asadi-Aliabadi, M., Asadi-Pooya, A.A., Ashbaugh, C., Assmus, M., Atafar, Z., Atnafu, D.D., Atout, M.M.W., Ausloos, F., Ausloos, M., Ayala Quintanilla, B.P., Ayano, G., Ayanore, M.A., Azari, S., Azarian, G., Azene, Z.N., Badawi, A., Badiye, A.D., Bahrami, M.A., Bakhshaei, M.H., Bakhtiari, A., Bakkannavar, S.M., Baldasseroni, A., Ball, K., Ballew, S.H., Balzi, D., Banach, M., Banerjee, S.K., Bante, A.B., Baraki, A.G., Barker-Collo, S.L., Bärnighausen, T.W., Barrero, L.H., Barthelemy, C.M., Barua, L., Basu, S., Baune, B.T., Bayati, M., Becker, J.S., Bedi, N., Beghi, E., Béjot, Y., Bell, M.L., Bennitt, F.B., Bensenor, I.M., Berhe, K., Berman, A.E., Bhagavathula, A.S., Bhageerathy, R., Bhala, N., Bhandari, D., Bhattacharyya, K., Bhutta, Z.A., Bijani, A., Bikbov, B., Bin Sayeed, M.S., Biondi, A., Birihane, B.M., Bisignano, C., Biswas, R.K., Bitew, H., Bohlouli, S., Bohluli, M., Boon-Dooley, A.S., Borges, G., Borzì, A.M., Borzouei, S., Bosetti, C., Boufous, S., Braithwaite, D., Breitborde, N.J.K., Breitner, S., Brenner, H., Briant, P.S., Briko, A.N., Briko, N.I., Britton, G.B., Bryazka, D., Bumgarner, B.R., Burkart, K., Burnett, R.T., Burugina Nagaraja, S., Butt, Z.A., Caetano dos Santos, F.L., Cahill, L.E., Cámera, L.L.A., Campos-Nonato, I.R., Cárdenas, R., Carreras, G., Carrero, J.J., Carvalho, F., Castaldelli-Maia, J.M., Castañeda-Orjuela, C.A., Castelpietra, G., Castro, F., Causey, K., Cederroth, C.R., Cercy, K.M., Cerin, E., Chandan, J.S., Chang, K.-L., Charlson, F.J., Chattu, V.K., Chaturvedi, S., Cherbuin, N., Chimed-Ochir, O., Cho, D.Y.,

Choi, J.-Y.J., Christensen, H., Chu, D.-T., Chung, M.T., Chung, S.-C., Cicuttini, F.M., Ciobanu, L.G., Cirillo, M., Classen, T.K.D., Cohen, A.J., Compton, K., Cooper, O.R., Costa, V.M., Cousin, E., Cowden, R.G., Cross, D.H., Cruz, J.A., Dahlawi, S.M.A., Damasceno, A.A.M., Damiani, G., Dandona, L., Dandona, R., Dangel, W.J., Danielsson, A.-K., Dargan, P.I., Darwesh, A.M., Daryani, A., Das, J.K., Das Gupta, R., das Neves, J., Dávila-Cervantes, C.A., Davitoiu, D.V., De Leo, D., Degenhardt, L., DeLang, M., Dellavalle, R.P., Demeke, F.M., Demoz, G.T., Demsie, D.G., Denova-Gutiérrez, E., Dervenis, N., Dhungana, G.P., Dianatinasab, M., Dias da Silva, D., Diaz, D., Dibaji Forooshani, Z.S., Djalalinia, S., Do, H.T., Dokova, K., Dorostkar, F., Doshmangir, L., Driscoll, T.R., Duncan, B.B., Duraes, A.R., Eagan, A.W., Edvardsson, D., El Nahas, N., El Sayed, I., El Tantawi, M., Elbarazi, I., Elgendy, I.Y., El-Jaafary, S.I., Elyazar, I.R., Emmons-Bell, S., Erskine, H.E., Eskandarieh, S., Esmaeilnejad, S., Esteghamati, A., Estep, K., Etemadi, A., Etisso, A.E., Fanzo, J., Farahmand, M., Fareed, M., Faridnia, R., Farioli, A., Faro, A., Faruque, M., Farzadfar, F., Fattahi, N., Fazlzadeh, M., Feigin, V.L., Feldman, R., Fereshtehnejad, S.-M., Fernandes, E., Ferrara, G., Ferrari, A.J., Ferreira, M.L., Filip, I., Fischer, F., Fisher, J.L., Flor, L.S., Foigt, N.A., Folayan, M.O., Fomenkov, A.A., Force, L.M., Foroutan, M., Franklin, R.C., Freitas, M., Fu, W., Fukumoto, T., Furtado, J.M., Gad, M.M., Gakidou, E., Gallus, S., Garcia-Basteiro, A.L., Gardner, W.M., Geberemariyam, B.S., Gebreslassie, A.A.A.A., Geremew, A., Gershberg Hayoon, A., Gething, P.W., Ghadimi, M., Ghadiri, K., Ghaffarifar, F., Ghafourifard, M., Ghamari, F., Ghashghaee, A., Ghiasvand, H., Ghith, N., Gholamian, A., Ghosh, R., Gill, P.S., Ginindza, T.G.G., Giussani, G., Gnedovskaya, E.V., Goharinezhad, S., Gopalani, S.V., Gorini, G., Goudarzi, H., Goulart, A.C., Greaves, F., Grivna, M., Grosso, G., Gubari, M.I.M., Gugnani, H.C., Guimarães, R.A., Guled, R.A., Guo, G., Guo, Y., Gupta, R., Gupta, T., Haddock, B., Hafezi-Nejad, N., Hafiz, A., Haj-Mirzaian, Arvin, Haj-Mirzaian, Arya, Hall, B.J., Halvaei, I., Hamadeh, R.R., Hamidi, S., Hammer, M.S., Hankey, G.J., Haririan, H., Haro, J.M., Hasaballah, A.I., Hasan, M.M., Hasanpoor, E., Hashi, A., Hassanipour, S., Hassankhani, H., Havmoeller, R.J., Hay, S.I., Hayat, K., Heidari, G., Heidari-Soureshjani, R., Henrikson, H.J., Herbert, M.E., Herteliu, C., Heydarpour, F., Hird, T.R., Hoek, H.W., Holla, R., Hoogar, P., Hosgood, H.D., Hossain, N., Hosseini, M., Hosseinzadeh, M., Hostiuc, M., Hostiuc, S., Househ, M., Hsairi, M., Hsieh, V.C., Hu, G., Hu, K., Huda, T.M., Humayun, A., Huynh, C.K., Hwang, B.-F., Iannucci, V.C., Ibitoye, S.E., Ikeda, N., Ikuta, K.S., Ilesanmi, O.S., Ilic, I.M., Ilic, M.D., Inbaraj, L.R., Ippolito, H., Iqbal, U., Irvani, S.S.N., Irvine, C.M.S., Islam, M.M., Islam, S.M.S., Iso, H., Ivers, R.Q., Iwu, C.C.D., Iwu, C.J., Iyamu, I.O., Jaafari, J., Jacobsen, K.H., Jafari, H., Jafarinia, M., Jahani, M.A., Jakovljevic, M., Jalilian, F., James, S.L., Janjani, H., Javaheri, T., Javidnia, J., Jeemon, P., Jenabi, E., Jha, R.P., Jha, V., Ji, J.S., Johansson, L., John, O., John-Akinola, Y.O., Johnson, C.O., Jonas, J.B., Joukar, F., Jozwiak, J.J., Jürisson, M., Kabir, A., Kabir, Z., Kalani, H., Kalani, R., Kalankesh, L.R., Kalhor, R., Kanchan, T., Kapoor, N., Karami Matin, B., Karch, A., Karim, M.A., Kassa, G.M., Katikireddi, S.V., Kayode, G.A., Kazemi Karyani, A., Keiyoro, P.N., Keller, C., Kemmer, L., Kendrick, P.J., Khalid, N., Khammarnia, M., Khan, E.A., Khan, M., Khatab, K., Khater, M.M., Khatib, M.N., Khayamzadeh, M., Khazaei, S., Kieling, C., Kim, Y.J., Kimokoti, R.W., Kisa, A., Kisa, S., Kivimäki, M., Knibbs, L.D., Knudsen, A.K.S., Kocarnik, J.M., Kochhar, S., Kopec, J.A., Korshunov, V.A., Koul, P.A., Koyanagi, A., Kraemer, M.U.G., Krishan, K., Krohn, K.J., Kromhout, H., Kuate Defo, B., Kumar, G.A., Kumar, V., Kurmi, O.P., Kusuma, D., La Vecchia, C., Lacey, B., Lal, D.K., Lalloo, R., Lallukka, T., Lami, F.H., Landires, I., Lang, J.J., Langan, S.M., Larsson, A.O., Lasrado, S., Lauriola, P., Lazarus, J.V., Lee, P.H., Lee, S.W.H., LeGrand, K.E., Leigh, J., Leonardi, M., Lescinsky, H., Leung, J., Levi, M., Li, S., Lim, L.-L., Linn, S., Liu, Shiwei, Liu, Simin, Liu, Y., Lo, J., Lopez, A.D., Lopez, J.C.F., Lopukhov, P.D., Lorkowski, S., Lotufo, P.A., Lu, A., Lugo, A., Maddison, E.R., Mahasha, P.W., Mahdavi, M.M., Mahmoudi, M., Majeed, A., Maleki, A., Maleki, S., Malekzadeh, R., Malta, D.C., Mamun, A.A., Manda, A.L., Manguerra, H., Mansour-Ghanaei, F., Mansouri, B., Mansournia, M.A., Mantilla Herrera, A.M., Maravilla, J.C., Marks, A., Martin, R.V., Martini, S., Martins-Melo, F.R., Masaka, A., Masoumi, S.Z., Mathur, M.R., Matsushita, K., Maulik, P.K., McAlinden, C., McGrath, J.J., McKee, M., Mehndiratta, M.M., Mehri, F., Mehta, K.M., Memish, Z.A., Mendoza, W., Menezes, R.G., Mengesha, E.W., Mereke, A., Mereta, S.T., Meretoja, A., Meretoja, T.J., Mestrovic, T., Miazgowski, B., Miazgowski, T., Michalek, I.M., Miller, T.R., Mills, E.J., Mini, G., Miri, M., Mirica, A., Mirrakhimov, E.M., Mirzaei, H., Mirzaei, M., Mirzaei, R., Mirzaei-Alavijeh, M., Misganaw, A.T., Mithra, P., Moazen, B., Mohammad, D.K., Mohammad, Y., Mohammad Gholi Mezerji, N., Mohammadian-Hafshejani, A., Mohammadifard, N., Mohammadpourhodki, R., Mohammed, A.S., Mohammed, H., Mohammed, J.A., Mohammed, S., Mokdad, A.H., Molokhia, M., Monasta, L., Mooney, M.D., Moradi, G., Moradi, M., Moradi-Lakeh, M., Moradzadeh, R., Moraga, P., Morawska, L., Morgado-da-Costa, J., Morrison, S.D., Mosapour, A., Mosser, J.F., Mouodi, S., Mousavi, S.M., Mousavi Khaneghah, A., Mueller, U.O., Mukhopadhyay, S., Mullany, E.C., Musa, K.I., Muthupandian, S., Nabhan, A.F., Naderi, M., Nagarajan, A.J., Nagel, G., Naghavi, M., Naghshtabrizi, B., Naimzada, M.D., Najafi, F., Nangia, V., Nansseu, J.R., Naserbakht, M., Nayak, V.C., Negoi, I., Ngunjiri, J.W., Nguyen, C.T., Nguyen, H.L.T., Nguyen, M., Nigatu, Y.T., Nikbakhsh, R., Nixon, M.R., Nnaji, C.A., Nomura, S., Norrving, B., Noubiap, J.J., Nowak, C., Nunez-Samudio, V., Oţoiu, A., Oancea, B., Odell, C.M., Ogbo, F.A., Oh, I.-H., Okunga, E.W., Oladnabi, M., Olagunju, A.T., Olusanya, B.O., Olusanya, J.O., Omer, M.O., Ong, K.L., Onwujekwe, O.E., Orpana, H.M., Ortiz, A., Osarenotor, O., Osei, F.B., Ostroff, S.M., Otstavnov, N., Otstavnov, S.S., Øverland, S., Owolabi, M.O., P A, M., Padubidri, J.R., Palladino, R., Panda-Jonas, S., Pandey, A., Parry, C.D.H., Pasovic, M., Pasupula, D.K., Patel, S.K., Pathak, M., Patten, S.B., Patton, G.C., Pazoki Toroudi, H., Peden, A.E., Pennini, A., Pepito, V.C.F., Peprah, E.K., Pereira, D.M., Pesudovs, K., Pham, H.Q., Phillips, M.R., Piccinelli, C., Pilz, T.M., Piradov, M.A., Pirsaheb, M., Plass, D., Polinder, S., Polkinghorne, K.R., Pond, C.D., Postma, M.J., Pourjafar, H., Pourmalek, F., Poznańska, A., Prada, S.I., Prakash, V., Pribadi, D.R.A., Pupillo, E., Quazi Syed, Z., Rabiee, M., Rabiee, N., Radfar, A., Rafiee, A., Raggi, A., Rahman, M.A., Rajabpour-Sanati, A., Rajati, F., Rakovac, I., Ram, P., Ramezanzadeh, K., Ranabhat, C.L., Rao, P.C., Rao, S.J., Rashedi, V., Rathi, P., Rawaf, D.L., Rawaf, S., Rawal, L., Rawassizadeh, R., Rawat, R., Razo, C., Redford, S.B., Reiner, R.C., Reitsma, M.B., Remuzzi, G., Renjith, V., Renzaho, A.M.N., Resnikoff, S., Rezaei, Negar, Rezaei, Nima, Rezapour, A., Rhinehart, P.-A., Riahi, S.M., Ribeiro, D.C., Ribeiro, D., Rickard, J., Rivera, J.A., Roberts, N.L.S., Rodríguez-Ramírez, S., Roever, L., Ronfani, L., Room, R., Roshandel, G., Roth, G.A., Rothenbacher, D., Rubagotti, E., Rwegerera, G.M., Sabour, S., Sachdev, P.S., Saddik, B., Sadeghi, E., Sadeghi, M., Saeedi, R., Saeedi Moghaddam, S., Safari, Y., Safi, S., Safiri, S., Sagar, R., Sahebkar, A., Sajadi, S.M., Salam, N., Salamati, P., Salem, H., Salem, M.R.R., Salimzadeh, H., Salman, O.M., Salomon, J.A., Samad, Z., Samadi Kafil, H., Sambala, E.Z., Samy, A.M., Sanabria, J., Sánchez-Pimienta, T.G., Santomauro, D.F., Santos, I.S., Santos, J.V., Santric-Milicevic, M.M., Saraswathy, S.Y.I., Sarmiento-Suárez, R., Sarrafzadegan, N., Sartorius, B., Sarveazad, A., Sathian, B., Sathish, T., Sattin, D., Saxena, S., Schaeffer, L.E., Schiavolin, S., Schlaich, M.P., Schmidt, M.I., Schutte, A.E., Schwebel, D.C., Schwendicke, F., Senbeta, A.M., Senthilkumaran, S., Sepanlou, S.G., Serdar, B., Serre, M.L., Shadid, J., Shafaat, O., Shahabi, S., Shaheen, A.A., Shaikh, M.A., Shalash, A.S., Shams-Beyranvand, M., Shamsizadeh, M., Sharafi, K., Sheikh, A., Sheikhtaheri, A., Shibuya, K., Shield, K.D., Shigematsu, M., Shin, J.I., Shin, M.-J., Shiri, R., Shirkoohi, R., Shuval, K., Siabani, S., Sierpinski, R., Sigfusdottir, I.D., Sigurvinsdottir, R., Silva, J.P., Simpson, K.E., Singh, J.A., Singh, P., Skiadaresi, E., Skou, S.T.S., Skryabin, V.Y., Smith, E.U.R., Soheili, A., Soltani, S., Soofi, M., Sorensen, R.J.D., Soriano, J.B., Sorrie, M.B., Soshnikov, S., Soyiri, I.N., Spencer, C.N., Spotin, A., Sreeramareddy, C.T., Srinivasan, V., Stanaway, J.D., Stein, C., Stein, D.J., Steiner, C., Stockfelt, L., Stokes, M.A., Straif, K., Stubbs, J.L., Sufiyan, M.B., Suleria, H.A.R., Suliankatchi Abdulkader, R., Sulo, G., Sultan, I., Szumowski, Ł., Tabarés-Seisdedos, R., Tabb, K.M., Tabuchi, T., Taherkhani, A., Tajdini, M., Takahashi, K., Takala, J.S., Tamiru, A.T., Taveira, N., Tehrani-Banihashemi, A., Temsah, M.-H., Tesema, G.A., Tessema, Z.T., Thurston, G.D., Titova, M.V., Tohidinik, H.R., Tonelli, M., Topor-Madry, R., Topouzis, F., Torre, A.E., Touvier, M., Tovani-Palone, M.R.R., Tran, B.X., Travillian, R., Tsatsakis, A., Tudor Car, L., Tyrovolas, S., Uddin, R., Umeokonkwo, C.D., Unnikrishnan, B., Upadhyay, E., Vacante, M., Valdez, P.R., van Donkelaar, A., Vasankari, T.J., Vasseghian, Y., Veisani, Y., Venketasubramanian, N., Violante, F.S., Vlassov, V., Vollset, S.E., Vos, T., Vukovic, R., Waheed, Y., Wallin, M.T., Wang, Y., Wang, Y.-P., Watson, A., Wei, J., Wei, M.Y.W., Weintraub, R.G., Weiss, J., Werdecker, A., West, J.J., Westerman, R., Whisnant, J.L., Whiteford, H.A., Wiens, K.E., Wolfe, C.D.A., Wozniak, S.S., Wu, A.-M., Wu, J., Wulf Hanson, S., Xu, G., Xu, R., Yadgir, S., Yahyazadeh Jabbari, S.H., Yamagishi, K., Yaminfirooz, M., Yano, Y., Yaya, S., Yazdi-Feyzabadi, V., Yeheyis, T.Y., Yilgwan, C.S., Yilma, M.T., Yip, P., Yonemoto, N., Younis, M.Z., Younker, T.P., Yousefi, B., Yousefi, Z., Yousefinezhadi, T., Yousuf, A.Y., Yu, C., Yusefzadeh, H., Zahirian Moghadam, T., Zamani, M., Zamanian, M., Zandian, H., Zastrozhin, M.S., Zhang, Y., Zhang, Z.-J., Zhao, J.T., Zhao, X.-J.G., Zhao, Y., Zhou, M., Ziapour, A., Zimsen, S.R.M., Brauer, M., Afshin, A., Lim, S.S., 2020. Global burden of 87 risk factors in 204 countries and territories, 1990–2019: a systematic analysis for the Global Burden of Disease Study 2019. The Lancet 396, 1223–1249. https://doi.org/10.1016/S0140-6736(20)30752-2

Wei, J., Huang, W., Li, Z., Xue, W., Peng, Y., Sun, L., Cribb, M., 2019. Estimating 1-km-resolution PM2.5 concentrations across China using the space-time random forest approach. Remote Sensing of Environment 231, 111221. https://doi.org/10.1016/j.rse.2019.111221

Wei, J., Li, Z., Cribb, M., Huang, W., Xue, W., Sun, L., Guo, J., Peng, Y., Li, J., Lyapustin, A., Liu, L., Wu, H., Song, Y., 2020. Improved 1 km resolution PM_{2.5} estimates across China using enhanced space–time extremely randomized trees. Atmos. Chem. Phys. 20, 3273–3289. https://doi.org/10.5194/acp-20-3273-2020

Wei, J., Li, Z., Lyapustin, A., Sun, L., Peng, Y., Xue, W., Su, T., Cribb, M., 2021. Reconstructing 1-km-resolution high-quality PM2.5 data records from 2000 to 2018 in China: spatiotemporal variations and policy implications. Remote Sensing of Environment 252, 112136. https://doi.org/10.1016/j.rse.2020.112136

Zhan, Y., Luo, Y., Deng, X., Grieneisen, M.L., Zhang, M., Di, B., 2018. Spatiotemporal prediction of daily ambient ozone levels across China using random forest for human exposure assessment. Environmental Pollution 233, 464–473. https://doi.org/10.1016/j.envpol.2017.10.029

Zhao, C., Wang, Q., Ban, J., Liu, Z., Li, T., 2019. Estimating the daily PM2.5 concentration in the Beijing-Tianjin-Hebei region using a random forest model with a 0.01° × 0.01° spatial resolution. Environment international 134, 105297.